Crystal Structure, Electronic Structure, and Physical Properties of Two New Antimonide−Tellurides: ZrSbTe and HfSbTe

Navid Soheilnia, Katja M. Kleinke, and Holger Kleinke*

Department of Chemistry, University of Waterloo, Waterloo, Ontario, Canada N2L 3G1

Received November 13, 2006. Revised Manuscript Received January 17, 2007

The isostructural title compounds were prepared from the elements in the stoichiometric ratio at 700 °C under exclusion of air. ZrSbTe and HfSbTe crystallize in the orthorhombic space group *Immm*, NbPS type, $Z = 4$, with $a = 3.91171(6)$ Å, $b = 5.80593(8)$ Å, $c = 13.4630(3)$ Å, $V = 305.760(6)$ Å^3 for ZrSbTe, and $a = 3.86757(8)$ Å, $b = 5.75115(9)$ Å, $c = 13.4422(3)$ Å, $V = 298.995(6)$ Å^3 for HfSbTe. The transition metal atoms are surrounded by four Sb and four Te atoms in the form of a bicapped trigonal prism. Two such prisms are joined via the third rectangular face, yielding a metal−metal bond across this face. The structures bestow with their unusual rectangular planar Sb layers exhibiting nonclassical Sb−Sb bonding. The distortion within the layers, reflected in the formation of alternating Sb−Sb distances along the *b*-axis, occurs with the formation of a band gap within the Sb bands. However, both compounds are metallic conductors with a small Seebeck coefficient, a consequence of a partial overlap of metal and Te states caused by the metal−metal bond.

Introduction

Several new transition metal antimonide−chalcogenides were introduced during the last seven years, including a new superconductor, Mo_2SbS_2,[1] new layered materials with large cavities, $MoSb_2S$[2] and $MoSb_2Se$,[3,4] and a new thermoelectric material, $Mo_3Sb_{5+\delta}Te_{2-\delta}$.[5−7] In the search for new thermoelectrics, DiSalvo and co-workers found the metallic Ni-rich chalcogenides Ni_2SbTe_2,[8] $Ni_{5.66}SbTe_2$, and $Ni_{5.75}SbSe_2$.[9] The structures of these materials (with the exception of the Ni-rich compounds) all fascinate the researcher because of their various nonclassical Sb−Sb interactions, e.g., bonds of the order of 3.0−3.2 Å typically classified as half bonds.[10−14] Notably, the group 4 antimonides $ZrSb_2$ and $HfSb_2$ are comprised of such interactions as well, as in detail discussed by Hoffmann and co-worker,[15] and the recently introduced Hf_5Sb_9 constitutes the first example of a so-called "T net", wherein each Sb atom is connected to three Sb neighbors in form of a "T", like Br to Cl in $BrCl_3$.[16]

With respect to group 4 antimonide−chalcogenides, only one vague report about a "Zr_xSb_2Te" forming the ZrSiS type, thus comprising a planar Sb square net, was published in 1969,[17] besides the metal-rich $Ti_5Sb_{2.2}Se_{0.8}$ without any noticeable Sb−Sb interactions.[18] With this contribution, we present the synthesis, structure, and physical properties of ZrSbTe and HfSbTe, two new antimonide−tellurides crystallizing in the NbPS structure type.[19]

Experimental Section

Synthesis and Analysis. The elements were used directly as starting materials, stored in an argon-filled glovebox (Zr: powder, −325 mesh, 98.5%; Hf: powder −100 mesh, 99.6%; Sb: powder, −100 mesh, 99.5%; Te: powder, −325 mesh, 99.99%, all from ALFA AESAR). HfSbTe was first encountered as a side product, when attempting to prepare hypothetical $Hf_5Sb_{9-\delta}Te_\delta$, to modify the electron concentration of the unusual T net of Sb atoms of Hf_5Sb_9.[16] This reaction started from the elements in the ratio of Hf:Sb:Te = 5:7:3, which were loaded into a ceramic crucible (Tamman from ALFA AESAR) and then sealed under vacuum in a fused silica tube. The tube was heated to 1250 °C in a resistance furnace and then slowly (1 °C/min) cooled to room temperature.

The sample was analyzed via X-ray powder diffraction utilizing the INEL powder diffractometer with position-sensitive detector. The powder diagram consisted of the reflections of Hf_5Sb_9 and several unknown peaks. After postulating the existence of the hitherto unknown HfSbTe in the structure of isoelectronic TiAsTe,[20]

* To whom correspondence should be addressed. E-mail: kleinke@uwaterloo.ca.

(1) Lee, C.-S.; Safa-Sefat, A.; Greedan, J. E.; Kleinke, H. *Chem. Mater.* **2003**, *15*, 780−786.
(2) Lee, C.-S.; Kleinke, H. *Eur. J. Inorg. Chem.* **2002**, 591−596.
(3) Kleinke, H. *Chem. Commun.* **2000**, 1941−1942.
(4) Soheilnia, N.; Kleinke, K. M.; Assoud, A.; Kleinke, H. *J. Mater. Chem.* **2004**, *14*, 2768−2774.
(5) Dashjav, E.; Szczepenowska, A.; Kleinke, H. *J. Mater. Chem.* **2002**, *12*, 345−349.
(6) Soheilnia, N.; Dashjav, E.; Kleinke, H. *Can. J. Chem.* **2003**, *81*, 1157−1163.
(7) Gascoin, F.; Rasmussen, J.; Snyder, G. J. *J. Alloys Compd.* **2007**, *427*, 324−329.
(8) Reynolds, T. K.; Kelley, R. F.; DiSalvo, F. J. *J. Alloys Compd.* **2004**, *366*, 136−144.
(9) Reynolds, T. K.; Bales, J. G.; DiSalvo, F. J. *Chem. Mater.* **2002**, *14*, 4746−4751.
(10) Brylak, M.; Jeitschko, W. *Z. Naturforsch. B* **1994**, *49*, 747−752.
(11) Brylak, M.; Jeitschko, W. *Z. Naturforsch. B* **1995**, *50*, 899−904.
(12) Ferguson, M. J.; Hushagen, R. W.; Mar, A. *J. Alloys Compd.* **1997**, *249*, 191−198.
(13) Kleinke, H. *Eur. J. Inorg. Chem.* **1998**, 1369−1375.
(14) Papoian, G. A.; Hoffmann, R. *Angew. Chem., Int. Ed.* **2000**, *39*, 2408−2448.
(15) Papoian, G.; Hoffmann, R. *J. Am. Chem. Soc.* **2001**, *123*, 6600−6608.
(16) Assoud, A.; Kleinke, K. M.; Soheilnia, N.; Kleinke, H. *Angew. Chem., Int. Ed.* **2004**, *43*, 5260−5262.
(17) Barthelat, J. C.; Jeannin, Y.; Rancurel, J. F. *C. R. Seances Acad. Sci. C* **1969**, *268*, 1756−1759.
(18) Kleinke, H. *J. Alloys Compd.* **2002**, *336*, 132−137.
(19) Donohue, P. C.; Bierstedt, P. E. *Inorg. Chem.* **1969**, *8*, 2690−2694.
(20) Huang, F. Q.; Flaschenriem, C.; Brazis, P.; Kannewurf, C. R.; Ibers, J. A. *Inorg. Chem.* **2003**, *42*, 3194−3198.

10.1021/cm062705r CCC: $37.00
Published on Web 02/20/2007

its synthesis was optimized. The best yields were obtained at a reaction temperature of 750 °C using a slight excess of antimony and tellurium, corresponding to 30.4 at. % Hf instead of the nominal 33.3 at. %. The same conditions led to the best yields (>95%) of ZrSbTe as well. Varying the Sb/Te ratio caused an increase of side products, namely, $ZrSb_2$, $ZrTe_2$, $HfSb_2$, or $HfTe_2$.

An EDX investigation (EDX: energy-dispersive analysis of X-rays) using an electron microscope (LEO 1530) with an additional EDX device (EDAX Pegasus 1200) was performed on selected ZrSbTe and HfSbTe crystals. No heteroelements, such as silicon stemming from the reaction container, were found. While the Sb:Te ratios remained constant from one crystal to another, the strong overlap of the Sb−L (3.604 keV) and Te−L peaks (3.769 keV) caused bias to the quantitative results.

Structure Determination. We were unable to obtain single crystals of suitable size for a single-crystal structure determination, even when attempting chemical transport reactions. Therefore, we decided to perform Rietveld refinements[21] using the GSAS program[22,23] via the graphical interface EXPGUI.[24] Data were collected with the INEL powder diffractometer at room temperature using Cu $K\alpha_1$ radiation over periods of 15 h. The samples were of the nominal compositions $M_{0.91}SbTe$ with M = Zr and Hf. A pseudo-Voigt function, composed of a convolution of Gaussian and Lorentzian functions,[25] was selected to describe the peak shapes, whose parameters were subsequently refined to obtain the best fit to the experimental peak shapes.

The parameters of the recently published arsenide TiAsTe,[20] space group *Immm*, were selected as a starting model. Therein, the As site (4 g) was filled with Sb and the Ti site (4j) with Zr and Hf, respectively. Since in both cases a smaller atom was replaced with a larger one, we manually increased the lattice parameters *a*, *b*, and *c* each by 5% before commencing the refinements. Thereafter, the refinements converged with residual values of $R_{wp} = 0.0507$ for ZrSbTe and $R_{wp} = 0.0614$ for HfSbTe. The (isotropic) displacement parameters of the transition metal atoms were somewhat larger than those of the others, in particular, in the case of ZrSbTe: $U(Zr) = 2.7 \times (U(Sb) + U(Te))/2$ and $U(Hf) = 1.3 \times (U(Sb) + U(Te))/2$. This might indicate deficiencies on the 4j site in accord with the observations made during the synthesis. Subsequent refinements of the occupancies of the M sites slightly lowered the residual values to $R_{wp} = 0.0501$ for ZrSbTe and $R_{wp} = 0.0612$ for HfSbTe, yielded inconspicuous displacement parameters, and final occupancy factors of 0.951(6) and 0.974(6), respectively. The deficiencies are of the order of 4−8 times their standard deviation, which may be considered significant. Details of the crystallographic investigations are given in Table 1, and atomic positions and displacement parameters are in Tables 2 and 3.

Electronic Structure Calculations. The band structure of the experimentally observed Sb atom layer was modeled via the Extended Hückel approach,[26,27] in comparison with its hypothetical undistorted variant, using the standard ionization potential and expansion parameters of Sb.[28] Self-consistent tight-binding *first principles* LMTO calculations (LMTO = linear muffin tin orbitals) using the atomic spheres approximation (ASA)[29,30] were performed on the whole crystal structure of HfSbTe. In the LMTO approach, the density functional theory is employed with the local density approximation (LDA) for the exchange correlation energy.[31] The following wave functions were used: for Hf 6s, 6p, 5d, and included via the downfolding technique[32] 5f; for Sb and Te 5s, 5p, 5d (downfolded), and 4f (downfolded). 621 independent *k* points of the first Brillouin zone were chosen via an improved tetrahedron method.[33] We calculated the integrated COHP values (ICOHPs, COHP = crystal orbital Hamilton populations)[34,35] for the various Sb−Sb interactions of the planar Sb atom layer.

Table 1. Crystallographic Data for $Zr_{0.95}SbTe$ and $Hf_{0.97}SbTe$

empirical formula	$Zr_{0.951(6)}SbTe$	$Hf_{0.974(6)}SbTe$
formula weight [gmol^{-1}]	336.11	423.22
temperature [K]	298	298
wavelength [Å]	1.54056	1.54056
space group	*Immm* (No. 71)	*Immm* (No. 71)
cell dimensions		
a [Å]	3.91171(6)	3.86757(8)
b [Å]	5.80593(8)	5.75115(9)
c [Å]	13.4630(3)	13.4422(3)
V [Å^3]	305.760(6)	298.995(6)
no. of formula units per cell	4	4
calculated density [g cm^{-3}]	7.30	9.40
range in 2θ [deg]	3−97	3−97
R_P, R_{wP}	0.0416, 0.0501	0.0531, 0.0612

Table 2. Atomic Positions, Isotropic Displacement Parameters, and Occupancy Factors of $Zr_{0.95}SbTe$

atom	site	x	y	z	U_{eq}/Å^2	occupancy
Zr	4j	1/2	0	0.1309(1)	0.002(1)	0.951(6) Zr
Sb	4g	0	0.2553(3)	0	0.0023(5)	1 Sb
Te	4i	0	0	0.2918(1)	0.0058(5)	1 Te

Physical Property Measurements. Since single crystals could not be prepared with sufficient sizes for property measurements, we (cold-)pressed parts of the two ground phase-pure samples into two bar-shaped pellets of the dimensions 6 × 1 × 1 [in mm]. The densities achieved were about 80% of the hypothetical densities as determined via X-ray diffraction. The Seebeck coefficient (thermopower, *S*) was determined with a commercial thermopower system (MMR Technologies). The electrical conductivity (σ) was measured by determining the voltage drops ΔV over a distance of 2 mm under dynamic vacuum employing a homemade device with a helium compressor. The resistances (*R*) were calculated from the voltage drops using Ohm's law, i.e., $R = \Delta V/I$, with I = current. We calculated σ(T) after measuring the lengths between the contacts, *L*, according to $\sigma = L/(AR)$, with the area $A = 1$ mm × 1 mm.

Results and Discussion

Crystal Structures. ZrSbTe and HfSbTe are isostructural with the recently published arsenide−telluride TiAsTe,[20] adopting the NbPS structure type. The crystal structure of HfSbTe is composed of two-dimensional HfTe slabs alternating with planar Sb layers along the *c*-axis (Figure 1). The

(21) von Dreele, R. B.; Jorgensen, J. D.; Windsor, C. G. *J. Appl. Crystallogr.* **1982**, *15*, 581−589.
(22) Larson, L. C.; Von Dreele, R. B. *Generalized Structural Analysis System (GSAS)*; LANSCE, MSH805; Los Alamos National Laboratory: Los Alamos, NM, 1995.
(23) Larson, A. C.; von Dreele, R. B. *GSAS-General Structure Analysis System*; Los Alamos National Laboratory: Los Alamos, NM, 2000.
(24) Toby, B. H. *J. Appl. Crystallogr.* **2001**, *34*, 210−213.
(25) Thompson, P.; Cox, D. E.; Hastings, J. B. *J. Appl. Crystallogr.* **1987**, *20*, 79−83.
(26) Hoffmann, R. *J. Chem. Phys.* **1963**, *39*, 1397−1412.
(27) Whangbo, M.-H.; Hoffmann, R. *J. Am. Chem. Soc.* **1978**, *100*, 6093−6098.
(28) Clementi, E.; Roetti, C. *At. Data Nucl. Data Tables* **1974**, *14*, 177−478.
(29) Andersen, O. K. *Phys. Rev. B* **1975**, *12*, 3060−3083.
(30) Skriver, H. L. *The LMTO Method*; Springer: Berlin, Germany, 1984.
(31) Hedin, L.; Lundqvist, B. I. *J. Phys. C* **1971**, *4*, 2064−2083.
(32) Lambrecht, W. R. L.; Andersen, O. K. *Phys. Rev. B* **1986**, *34*, 2439−2449.
(33) Blöchl, P. E.; Jepsen, O.; Andersen, O. K. *Phys. Rev. B* **1994**, *49*, 16223−16233.
(34) Dronskowski, R.; Blöchl, P. E. *J. Phys. Chem.* **1993**, *97*, 8617−8624.
(35) Landrum, G. A.; Dronskowski, R. *Angew. Chem., Int. Ed.* **2000**, *39*, 1560−1585.

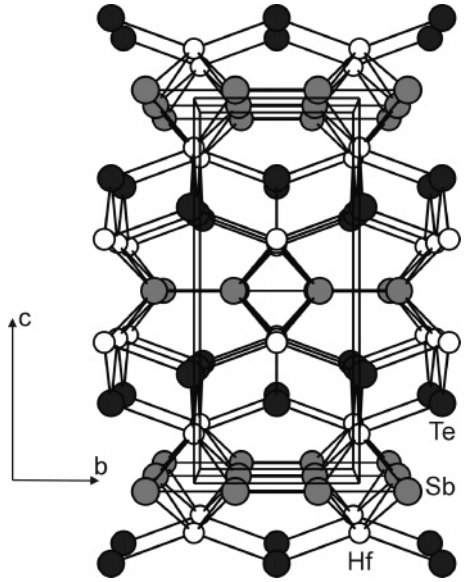

Figure 1. Crystal structure of HfSbTe in a projection along the *a*-axis.

Table 3. Atomic Positions, Isotropic Displacement Parameters, and Occupancy Factors of $Hf_{0.97}SbTe$

atom	site	x	y	z	U_{eq}/Å^2	occupancy
Hf	4j	1/2	0	0.1280(1)	0.0288(8)	0.974(6) Hf
Sb	4g	0	0.2620(4)	0	0.0250(8)	1 Sb
Te	4i	0	0	0.2925(1)	0.0252(8)	1 Te

Table 4. Selected Interatomic Distances [Å] of $Zr_{0.95}SbTe$ and $Hf_{0.97}SbTe$

	no.	ZrSbTe	HfSbTe
M−Sb	4×	3.021(2)	2.995(2)
M−Te	2×	2.919(2)	2.937(2)
M−Te	2×	3.0842(7)	3.0677(7)
M−M	1×	3.524(4)	3.442(3)
Sb−Sb	1×	2.842(4)	2.737(4)
Sb−Sb	1×	2.964(4)	3.014(4)

two different slabs are interconnected via covalent Hf−Sb interactions, resulting in a truly three-dimensional structure.

Thereby the Hf atoms are coordinated by four Sb atoms and two Te atoms at distances of 3.00 and 2.94 Å, respectively, in the form of a trigonal prism (Table 4). Two rectangular faces of the trigonal prism are capped by two additional Te atoms with Hf−Te distances of 3.07 Å. The third rectangular face is capped by an Hf atom resulting in an Hf−Hf distance of 3.44 Å, and two such prisms standing back to back along the *c*-axis. Each $HfSb_4Te_2$ prism is severely distorted, as the two Sb atoms form a bond of 3.01 Å, while the Sb−Te distances within the triangular face of the prism are 4.16 Å. The prisms form linear chains along the *a*-axis via condensation through opposing triangular faces. Last, the interconnection along the *b*-axis occurs by shared capping Te atoms as well as by the Sb−Sb interprism interactions of 2.74 Å.

Both the Hf−Sb and the Hf−Te distances are inconspicuous and compare well with those in the corresponding binaries. The analogous Zr−Sb and Zr−Te distances are overall slightly larger, in accord with the larger Pauling radius of Zr (1.45 Å), compared to Hf (1.44 Å),[36] which is also reflected in the larger unit cell volume of ZrSbTe.

(36) Pauling, L. *The Nature of the Chemical Bond*, 3rd ed.; Cornell University Press: Ithaca, NY, 1948.

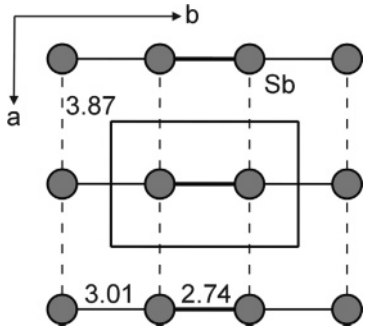

Figure 2. Sb atom layer of HfSbTe.

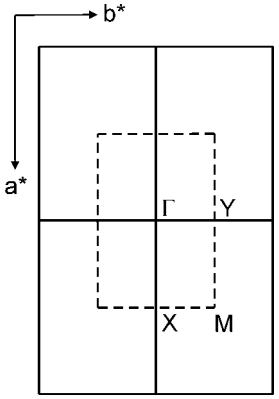

Figure 3. Four reciprocal unit cells (solid lines) of the Sb atom layer and the first Brillouin zone (dashed lines).

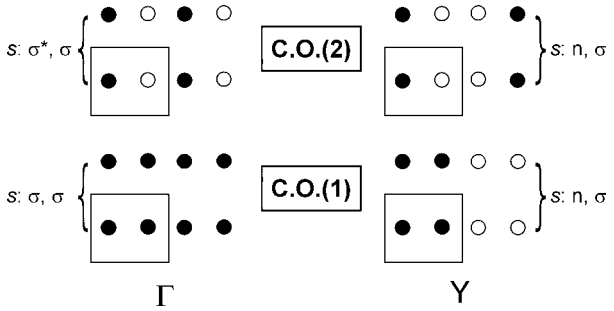

Figure 4. Crystal orbitals formed by the 5s orbitals of the regular Sb sheet at the zone center Γ (left) and the zone border Y (right).

Rather unusual, on the other hand, is the situation within the planar Sb sheet. Therein, Sb−Sb distances of 2.74 Å (interprism) and 3.01 Å (intraprism) alternate along the *b*-axis, and a much larger distance of 3.87 Å (i.e., the *a*-axis) occurs along the *a*-axis (Figure 2). Sb−Sb single-bond distances are usually about 2.8 Å,[3,37,38] and Sb−Sb distances of 3.0−3.1 Å are often considered to have a bond order of 1/2, i.e., correspond to half bonds.[10−14,39] Thus, the 3.87 Å interaction is expected to be very weak. Based on these distance values, 2.74 Å is a bit short for a single bond, and 3.01 Å could be classified as a half bond. The analogous distances of ZrSbTe are 2.84 Å, normal for a single bond, and 2.96 Å, somewhat short for a half bond.

Similar linear chains were found in the metal-rich antimonides $Zr_{7.5}V_{5.5}Sb_{10}$ (alternating distances of 2.80 and 2.88

(37) Hönle, W.; von Schnering, H.-G. *Z. Kristallogr.* **1981**, *155*, 307−314.
(38) Korber, N.; Richter, F. *Angew. Chem., Int. Ed. Engl.* **1997**, *36*, 1512−1514.
(39) Bolloré, G.; Ferguson, M. J.; Hushagen, R. W.; Mar, A. *Chem. Mater.* **1995**, *7*, 2229−2231.

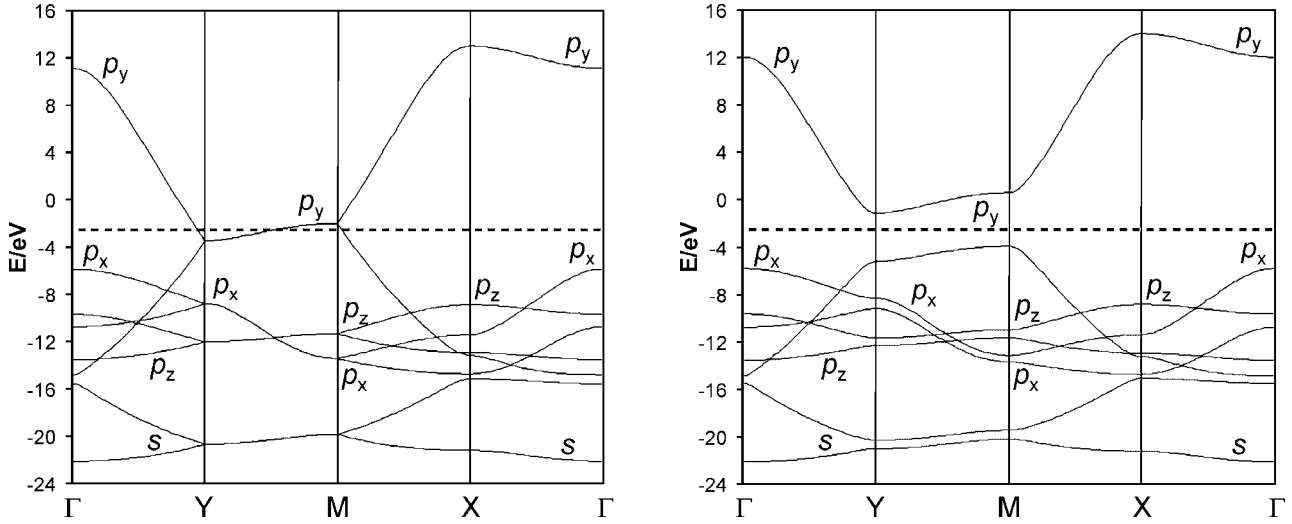

Figure 5. Band structures of planar Sb atom sheets, calculated using Extended Hückel. Left: hypothetical rectangular layer with distances of 2.88 Å along *b* and 3.87 Å along *a*. Right: layer as experimentally found in HfSbTe, depicted in Figure 2. Dashed horizontal lines depict the Fermi level, E_F, for seven valence electrons per Sb atom.

Å)[40] and $Zr_{7.5}V_{3.5}Sb_8$ (2.83 and 2.88 Å).[41] A double-chain (ladder) with equidistant Sb atoms along the chain direction (distance of 2.84 Å) occurs in $Zr_{4.3}Ti_{2.7}Sb_7$, with interchain distances of 3.48 Å.[42] Electronic structure calculations performed in these materials revealed these bonds within the linear chains to be delocalized 1-electron-2-center bonds, i.e., half bonds, despite their short lengths.

Electronic Structure. Since the Hf−Hf distance is much longer than twice the radius of an Hf atom, one could postulate the existence of Hf^{4+}. Because there are no Te−Te interactions, Te might achieve its octet by being reduced to Te^{2-}. Then, one obtains seven valence electrons per Sb atom, according to $Hf^{4+}Sb^{2-}Te^{2-}$. Therefore, one electron per Sb atom remains available for the formation of the Sb−Sb bonds. To gain insight into the bonding situation of the Sb sheet of HfSbTe, its electronic structure was modeled using the Extended Hückel approximation. For comparison, the band structure of a hypothetical undistorted variant was calculated as well, exhibiting equidistant Sb−Sb distances along the *b*-axis of $b/2 = 2.88$ Å, retaining the distance of $a = 3.87$ Å along [100]. The two-dimensional first Brillouin zone is shown in Figure 3, wherein Γ denotes the origin, $X = a^*/2$, $Y = b^*/2$, and $M = a^*/2 + b^*/2$.

First, we consider the regular rectangular Sb array with equiatomic distances along the *b*-axis. With two Sb atoms per unit cell, there are two crystal orbitals formed from each of the four orbitals per Sb atom, s, p_x, p_y, and p_z. For example, the two s-based crystal orbitals would correspond to one in-phase combination of the two s atomic orbitals, C.O.(1), and one out-of-phase combination, C.O.(2). At the zone center, Γ, all reciprocal unit cells exhibit the some crystal orbitals, while the phases of these orbitals alternate along *b** from one cell to the other at the Y point (Figure 4). Hence, C.O.-(1) is much lower in energy than C.O.(2) at Γ because of its σ bonding character along the chain. On the other hand, C.O.-(1) and C.O.(2) are degenerate in energy at Y in the regular sheet and intermediate in energy between C.O.(1) and C.O.-(2) at Γ.

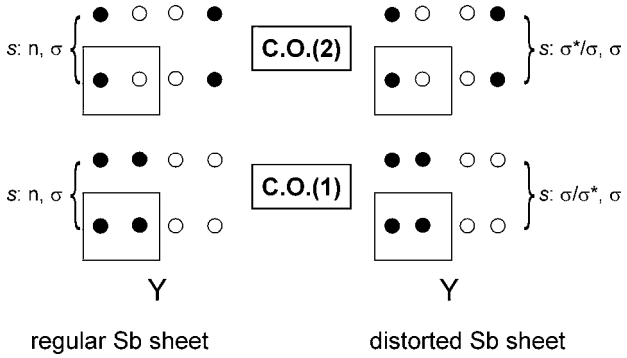

Figure 6. Impact of the experimentally observed distortion of the Sb sheet onto the crystal orbitals formed by the 5s orbitals at the zone border Y.

From Y to M, the corresponding bands remain degenerate, and the σ bonding character perpendicular to the chain direction changes into σ antibonding because of the phase change, i.e., the two bands run slightly uphill (Figure 5), as long as that interaction is significant.

That the interchain interaction is indeed significant is reflected in the different energies of the p_x and p_z orbitals because the only difference between the two is the interaction between the chains. This interaction is, at Γ, of σ* character for p_x and of π character for p_z. As the p_x-based bands are higher in energy at Γ, the interchain interaction is evidently noticeable, despite its length of 3.87 Å. The p_y-dominated bands exhibit intrachain σ character, and have thus the largest dispersion. At Γ, the p_y bonding combination is lower in energy than the lower p_x and p_z bands, while the antibonding σ intrachain interaction pushes the second p_y band toward much higher energies, causing a huge bandwidth of about 27 eV. Because of the s,p mixing,[43] the center of gravity of the p_y bands is higher than that of the p_x and p_z bands.

At seven valence electrons per Sb atom, corresponding to Sb^{2-}, the p_y bands are exactly half-filled (dashed horizontal

(40) Kleinke, H. *Chem. Commun.* **1998**, 2219−2220.
(41) Kleinke, H. *J. Mater. Chem.* **1999**, *9*, 2703−2708.
(42) Kleinke, H. *J. Am. Chem. Soc.* **2000**, *122*, 853−860.
(43) Ienco, A.; Hoffmann, R.; Papoian, G. *J. Am. Chem. Soc.* **2001**, *123*, 2317−2325.

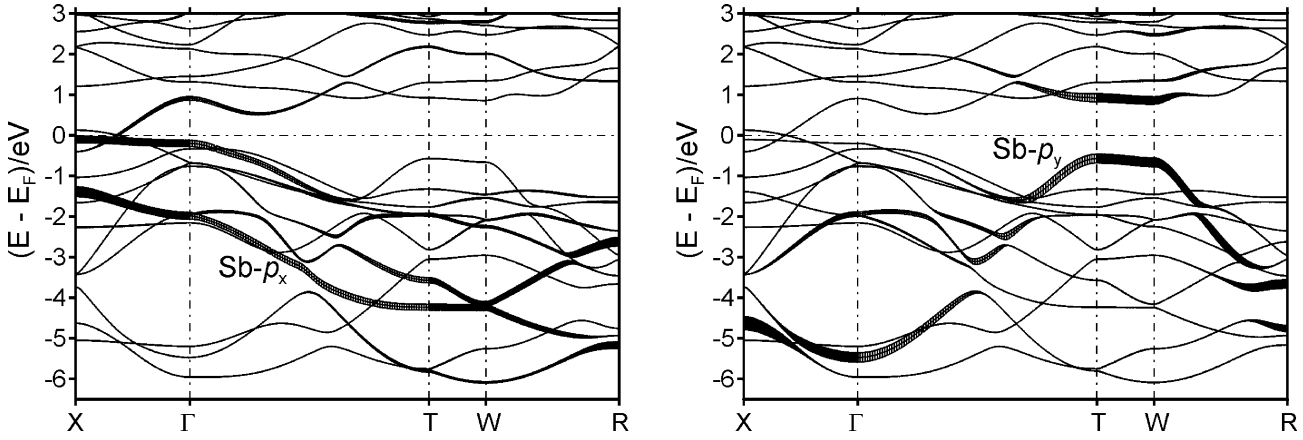

Figure 7. Band structure of HfSbTe, calculated via the LMTO method. Left: Sb p_x contributions; right: Sb p_y contributions emphasized via fat band representation. Dashed horizontal lines depict the Fermi level, E_F.

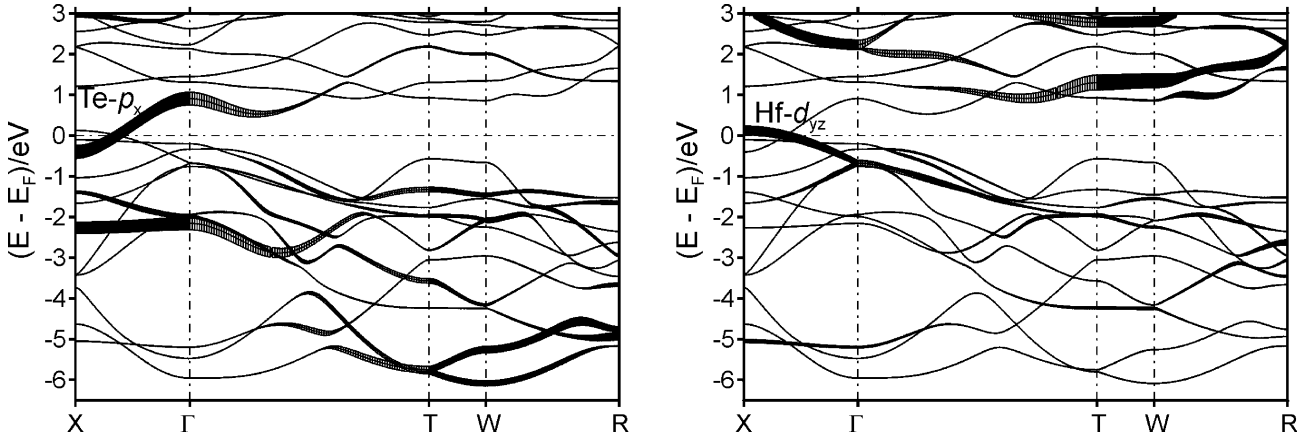

Figure 8. Band structure of HfSbTe, calculated via the LMTO method. Left: Te p_x contributions; right: Hf d_{yz} contributions emphasized via fat band representation. Dashed horizontal lines depict the Fermi level, E_F.

line in Figure 5), while all other bands are completely filled. This scenario causes two-dimensional metallic properties of the regular Sb array, as the p_y bands cross the Fermi level along $\Gamma \rightarrow$ Y and Y $\rightarrow$ M. Again, the latter crossing, i.e., the slight uphill slope along Y $\rightarrow$ M, is caused by the interchain interaction, which changes from weakly π bonding at Y to weakly π antibonding at M.

The most apparent difference between the band structures of the hypothetical regular and the experimentally observed (distorted) Sb sheets occurs at the points Y and M. In contrast to the regular sheet, the two p_y bands are not degenerate, reflected in a band gap opening at the Fermi level for seven valence electrons per Sb atom. Hence, the distortion may be regarded as a one-dimensional Peierls transition.

Moreover, neither of the p_x, p_z, and s bands are degenerate at these points in the distorted sheet, in contrast to the regular one. The effect of the distortion can be demonstrated by shifting one atomic orbital per cell of the regular sheet as depicted in Figure 4, i.e., by shortening one intrachain interaction combined with lengthening the next. That shift is reflected in a move of C.O.(1) toward lower energies because the bonding interaction along b is now shorter than the nonbonding one, while the opposite is true for C.O.(2). This is visualized in Figure 6, where the C.O.(1) orbitals drawn in black of the distorted sheet are closer to each other, compared to the distance between black and white of the same C.O.(1).

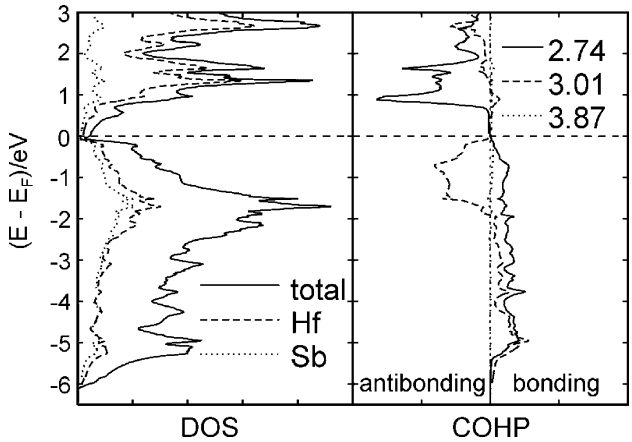

Figure 9. Densities of states (DOS, left) and Sb−Sb crystal orbital Hamilton populations (COHP, right). Dashed horizontal lines depict the Fermi level, E_F.

Below the gap, all π interactions along the chain are filled; i.e., bonding and antibonding π interactions cancel one another out. The σ bonding p_y band is also filled, and the σ antibonding band is the only empty one. In summary, one band of σ bonding character is responsible for the bonds within the chain of two Sb atoms, revealing both bonds to be delocalized 1-electron-2-center bonds, i.e., half bonds. Perpendicular to the chain direction, the amounts of empty p_y-based π bonding and antibonding states are the same, yielding an overall nonbonding interaction, or more precisely,

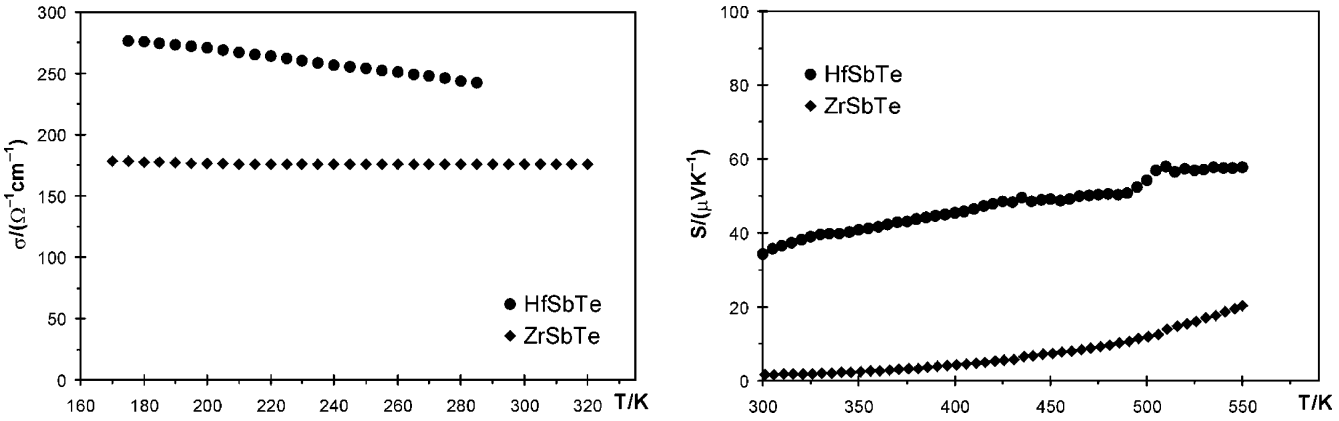

Figure 10. Electrical conductivity (left) and Seebeck coefficient (right) of ZrSbTe (diamonds) and HfSbTe (circles).

a slightly antibonding interaction, as antibonding contributions are more destabilizing than bonding ones stabilizing.

A comparison with the P atom sheet of superconducting NbPS is instructive. Hoffmann et al. presented the band structure for a hypothetical regular P layer,[44] where the *a* and *c* axes are interchanged compared to this work on HfSbTe. Then, the special points of the Brillouin zones are different as well, i.e., the M and X points shown here in Figure 3 are labeled T and Z, respectively, in the Brillouin zone of the P sheet. Its band structure shows strong resemblances, namely, the s, p_x, and p_z bands of the Sb layer are almost identical throughout the entire Brillouin zone. The major difference lies in the remaining bands of σ character along the chain direction. These bands occur at higher energies in the P layer because of the much stronger s,p mixing of the P atom, compared to Sb.

The band structure of the whole HfSbTe structure, as experimentally determined, is shown in Figure 7, with the Sb and Te s states occurring below the chosen energy window. The special points were chosen according to the standard for the orthorhombic body-centered case with $c > b > a$ (reciprocal space group *Fmmm*).[45] The Sb bands appear somewhat different, caused by covalent Hf−Sb mixing, but overall the slopes are comparable to those of the isolated Sb sheet. Figure 7 reveals the Sb p_x (left) and p_y (right) contributions via the fat band representation.[46]

As in the model of the distorted Sb^{2-} sheet, the Fermi level, E_F, falls into a gap between the Sb-based bands. However, two bands cross E_F along X → Γ, dominated by Te p_x and Hf d_{yz} states, respectively (Figure 8). Therefore, the Te states are partly empty and the Hf states partly filled, a consequence of the Hf−Hf interaction. In fact, its integrated COHP value was calculated to be −0.44 eV, quite significantly bonding. Hence, the description $Hf^{(4-\delta)+}Sb^{2-}Te^{(2-\delta)-}$ is more appropriate. Possibly most importantly, the band structure calculation suggests metallic properties.

With HfSbTe being metallic, and the Fermi level falling into a gap of the Sb-based bands, the question remains why the Sb sheet is distorted, i.e., why the interatomic distances within the Sb chain are not equidistant. The gap within the Sb states does not lead to semiconducting properties of HfSbTe, but it does occur with an energy gain, for the highest occupied states of the Sb sheet are lowered in energy. Steric reasons are unlikely to play a role, for an equidistant Sb chain would still give reasonable Hf−Sb and Sb−Te distances, changing from 3.00 and 3.66 Å to 2.96 and 3.69 Å.

Finally, the atomic projections onto the densities of states (DOS, left part of Figure 9) verify that the Sb contributions are the smallest at E_F and that only very few states are filled at E_F. Above E_F, the Hf d contributions clearly dominate. The Sb−Sb COHP curves (right part of Figure 9) are all zero at E_F, and the shortest Sb−Sb bond of 2.74 Å exhibits only bonding states below E_F, in contrast to the intermediate bond of 3.01 Å. However, both interactions are net bonding, as reflected in their negative ICOHP values of −1.16 eV for the 2.74 Å bond and −0.34 eV for the 3.01 Å bond. The COHP curve of the long interaction of 3.87 Å along the *c*-axis is barely visible, when plotted on the same scale like the shorter two. As predicted based on the Extended Hückel model of the Sb sheet, it is slightly antibonding, reflected in its small positive ICOHP value of +0.05 eV.

Physical Properties. The band structure calculation pointed toward (at least) one-dimensional metallic properties. Consequently, one expects the electrical conductivity to slowly decrease with increasing temperature. This is clearly the case for HfSbTe, reaching a room-temperature conductivity of 230 Ω^{-1} cm^{-1} (Figure 10), while the conductivity ZrSbTe (175 Ω^{-1} cm^{-1}) is basically independent of the temperature. It is noted that the actual specific conductivities are most likely higher because of the significant grain boundary effect stemming from the low densities of the samples. Moreover, the grain boundary effect also decreased the temperature dependence, for that effect is independent of the temperature, explaining the small slopes observed. As typical for metallic conductors, both ZrSbTe and HfSbTe exhibit a small Seebeck coefficient, i.e., +2 and +34 μV/K at 300 K, respectively, indicating that the p-type carriers dominate, a common observation in tellurides.

Conclusion

Two new materials, ZrSbTe and HfSbTe, were introduced with this contribution. Both crystallize in the NbPS structure type, exhibiting an unusual planar Sb atom layer. This layer is comprised of parallel chains with alternating distances of

(44) Keszler, D. A.; Hoffmann, R. *J. Am. Chem. Soc.* **1987**, *109*, 118−124.
(45) Bradley, C. J.; Cracknell, A. P. *The Mathematical Theory of Symmetry in Solids*; Clarendon Press: Oxford, 1972.
(46) Jepsen, O.; Andersen, O. K. *Z. Phys.* **1995**, *97*, 25.

2.74−2.84 and 2.96−3.01 Å and a larger interchain distance of 3.9 Å. Interestingly, the distortion of the layer occurs with a band gap opening within the Sb bands; however, the materials are metallic because of an overlap of metal d states with the Te p states, i.e., because of the presence of holes in the Te bands that are caused by the M−M bond. Therefore, such a material could become semiconducting if smaller or more electropositive M atoms while retaining the valence-electron concentration could be used.

Acknowledgment. Financial support from NSERC, CFI, OIT (Ontario Distinguished Researcher Award for H.K.), MMO, and the Canada Research Chair program (CRC for H.K.) is appreciated.

Supporting Information Available: Two plots depicting the Rietveld refinements on ZrSbTe and HfSbTe. This material is available free of charge via the Internet at http://pubs.acs.org.

CM062705R